Plunging to and escaping from a spherical orbit near a rotating black hole

Vladimír Karas

in collaboration with Ondřej Kopáček

Astronomical Institute, Czech Academy of Sciences

RAGtime 27, Opava, 10-14 November 2025

The model: rotating black hole

Kerr metric describing the geometry of the spacetime around the rotating black hole is expressed in Boyer-Lindquist coordinates $x^\mu = (t,\, r,\, \theta,\, \varphi)$ as follows (Misner et al. 1973):

$$ds^2 = -\frac{\Delta}{\Sigma}\left[dt - a\sin\theta\, d\varphi\right]^2 + \frac{\sin^2\theta}{\Sigma}\left[(r^2+a^2)d\varphi - a\, dt\right]^2 + \frac{\Sigma}{\Delta}\, dr^2 + \Sigma d\theta^2, \tag{1}$$

where

$$\Delta \equiv r^2 - 2Mr + a^2, \quad \Sigma \equiv r^2 + a^2\cos^2\theta. \tag{2}$$

Coordinate singularity at $\Delta = 0$ corresponds to outer/inner horizon of the black hole $r_\pm = M \pm \sqrt{M^2 - a^2}$. Rotation of the black hole is measured by the spin parameter $a \in \langle -M, M\rangle$. Here we only consider $a \geq 0$ without the loss of generality.

Spherical orbits: their stability and binding

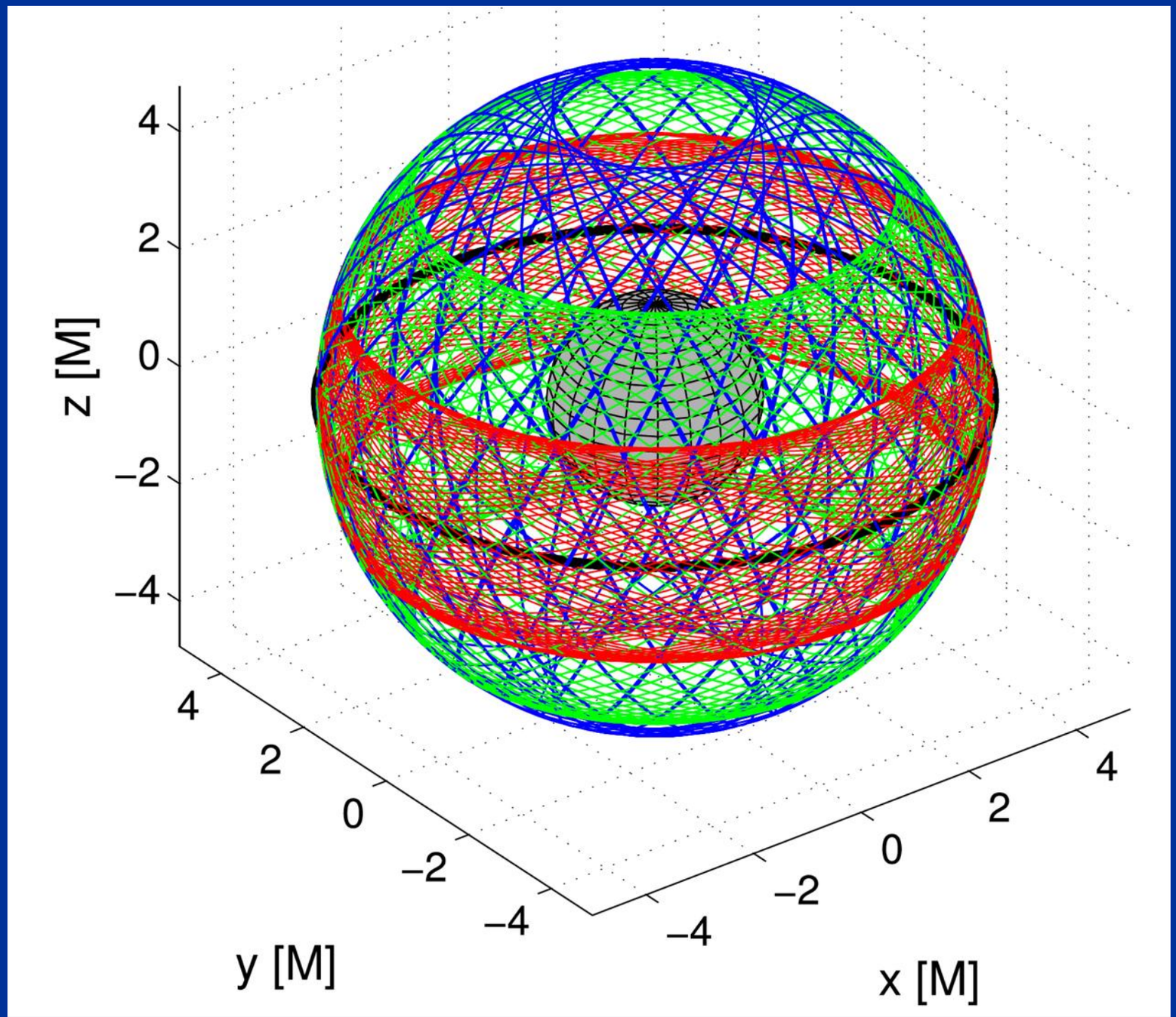

Geodesic motion in Kerr metric:

$a = 0.8$

$R = 5M$

$\Theta = 0, 1, 4, 9$

Kopáček & Karas, ApJ, 2024

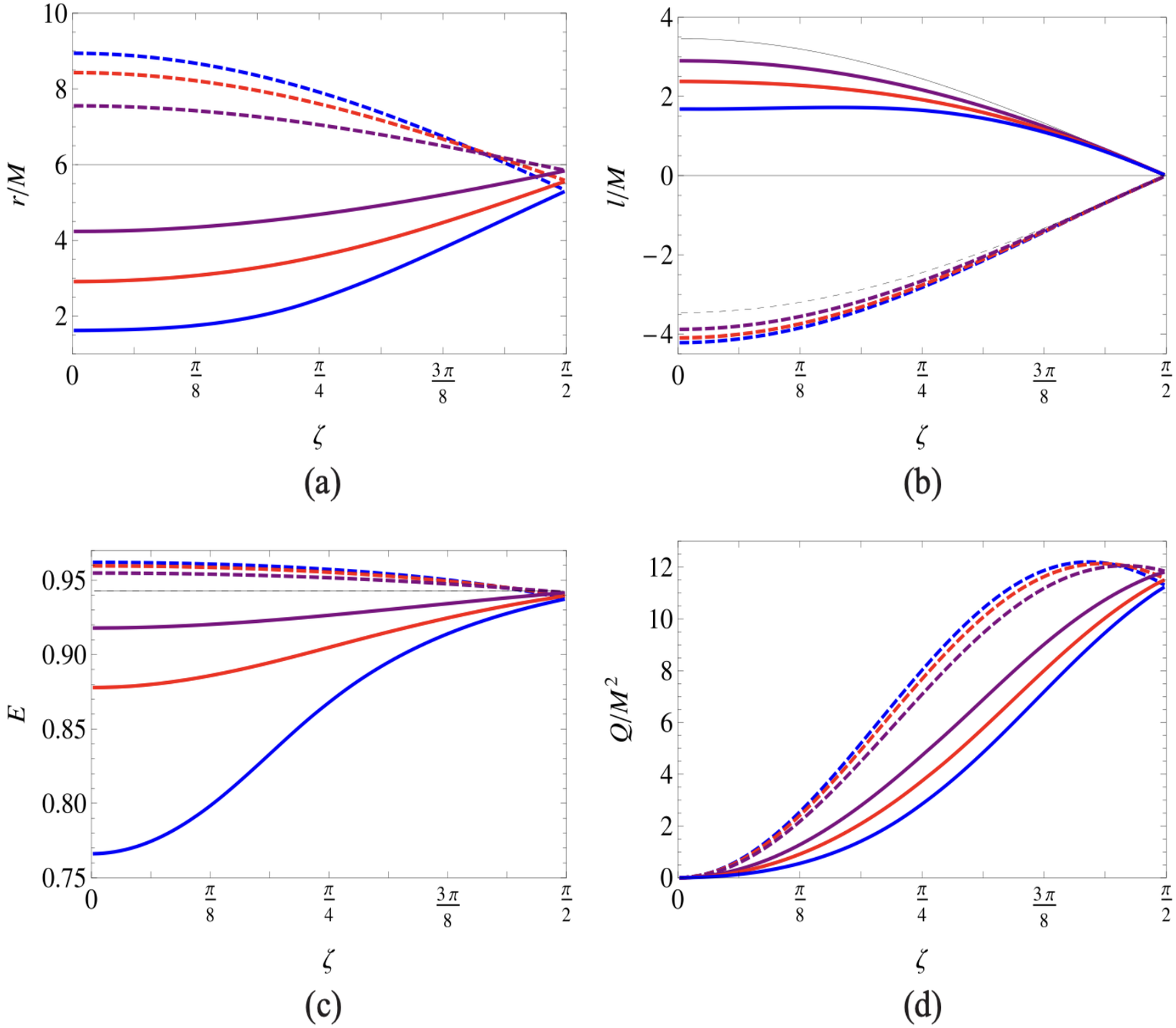

FIG. 4. Characteristic quantities of the ISSO as a function of the tilted angular ζ. (a) $r/M-\zeta$. (b) $l/M-\zeta$. (c) $E-\zeta$. (d) $Q/M^2-\zeta$. Black hole spin $a/M=-0.98,-0.8,-0.5,0.5,0.8,0.98$ for these thick curves from top to bottom in (a), (c), (d), and from bottom to top in (b). The solid thin curves are for the case with $a/M=0$. Dashed and solid curves are for the retrograde and prograde ISSOs.

We employ the test-field solution of Maxwell's equations for a weakly magnetized Kerr black hole immersed in an asymptotically uniform magnetic field specified by the component B_z parallel to the spin axis and the perpendicular component B_x. The electromagnetic vector potential A_μ is given as follows (Bičák & Janiš 1985):

$$A_t = \frac{B_z a M r}{\Sigma}\left(1+\cos^2\theta\right) - B_z a + \frac{B_x a M \sin\theta\cos\theta}{\Sigma}\left(r\cos\psi - a\sin\psi\right), \tag{3}$$

$$A_r = -B_x(r-M)\cos\theta\sin\theta\sin\psi, \tag{4}$$

$$A_\theta = -B_x a(r\sin^2\theta + M\cos^2\theta)\cos\psi - B_x(r^2\cos^2\theta - Mr\cos 2\theta + a^2\cos 2\theta)\sin\psi, \tag{5}$$

$$A_\varphi = B_z\sin^2\theta\left[\frac{1}{2}(r^2+a^2) - \frac{a^2 M r}{\Sigma}(1+\cos^2\theta)\right] \tag{6}$$

$$-B_x\sin\theta\cos\theta\left[\Delta\cos\psi + \frac{(r^2+a^2)M}{\Sigma}\left(r\cos\psi - a\sin\psi\right)\right],$$

where ψ denotes the azimuthal coordinate of Kerr ingoing coordinates, which is expressed in Boyer–Lindquist coordinates as follows:

$$\psi = \varphi + \frac{a}{r_+ - r_-}\ln\frac{r-r_+}{r-r_-}. \tag{7}$$

Conditions for the escape of charged particles

Effective potential expressing the minimal allowed energy of charged test particles in a non-axisymmetric magnetosphere of a rotating black hole may be derived in the rest frame of a static observer (Kopáček & Karas 2018c). Tetrad vectors of this frame are given as (Semerák 1993):

$$e^{\mu}_{(t)} = \left[\frac{\Sigma^{1/2}}{\chi}, 0, 0, 0\right], \quad e^{\mu}_{(r)} = \left[0, \frac{\Delta^{1/2}}{\Sigma^{1/2}}, 0, 0\right], \tag{10}$$

$$e^{\mu}_{(\theta)} = \left[0, 0, \frac{1}{\Sigma^{1/2}}, 0\right], \quad e^{\mu}_{(\varphi)} = \frac{\chi}{\sin\theta\Delta^{1/2}\Sigma^{1/2}}\left[\frac{-2aMr\sin^2\theta}{\chi^2}, 0, 0, 1\right], \tag{11}$$

where $\chi^2 \equiv \Delta - a^2\sin^2\theta$.

The static frame is employed to express the effective potential:

$$V_{\rm eff}(r,\theta,\varphi) = \left(-\beta + \sqrt{\beta^2 - 4\alpha\gamma}\right)/2\alpha, \tag{12}$$

with the coefficients defined as:

$$\alpha = \left[e^{t}_{(t)}\right]^2, \quad \beta = 2qA_t e^{t}_{(t)}, \quad \gamma = q^2\left[e^{t}_{(t)}\right]^2 A_t^2 - 1. \tag{13}$$

Escape in oblique configuration

Once the charge is introduced, the value of effective potential (12) changes accordingly. In order to study trajectories of escaping particles, we examine the behavior of the potential for $r \gg M$. In particular, for the initially neutral particle with energy $E_{\rm Kep}$ ionized in the equatorial plane at r_0 we obtain the following relation valid in the asymptotic region:

$$E - V_{\rm eff}|_{r\gg M} = E_{\rm Kep} - 1 - \frac{qB_z a}{r_0} + \mathcal{O}\left(r^{-1}\right). \tag{18}$$

Motion is possible only for $E \geq V_{\rm eff}$. Since $E_{\rm Kep} < 1$ with finite r_0 and $a \geq 0$ is considered, we observe that (i) particles may only escape for $qB_z < 0$, (ii) the escape is possible only for $a \neq 0$, (iii) asymptotic velocity of escaping particles is an increasing function of parameters $|qB_z|$ and a, and a decreasing function of r_0, and (iv) the escape is not allowed for the perpendicular inclination, $\alpha \equiv \arctan\left(B_x/B_z\right) = \pi/2$.

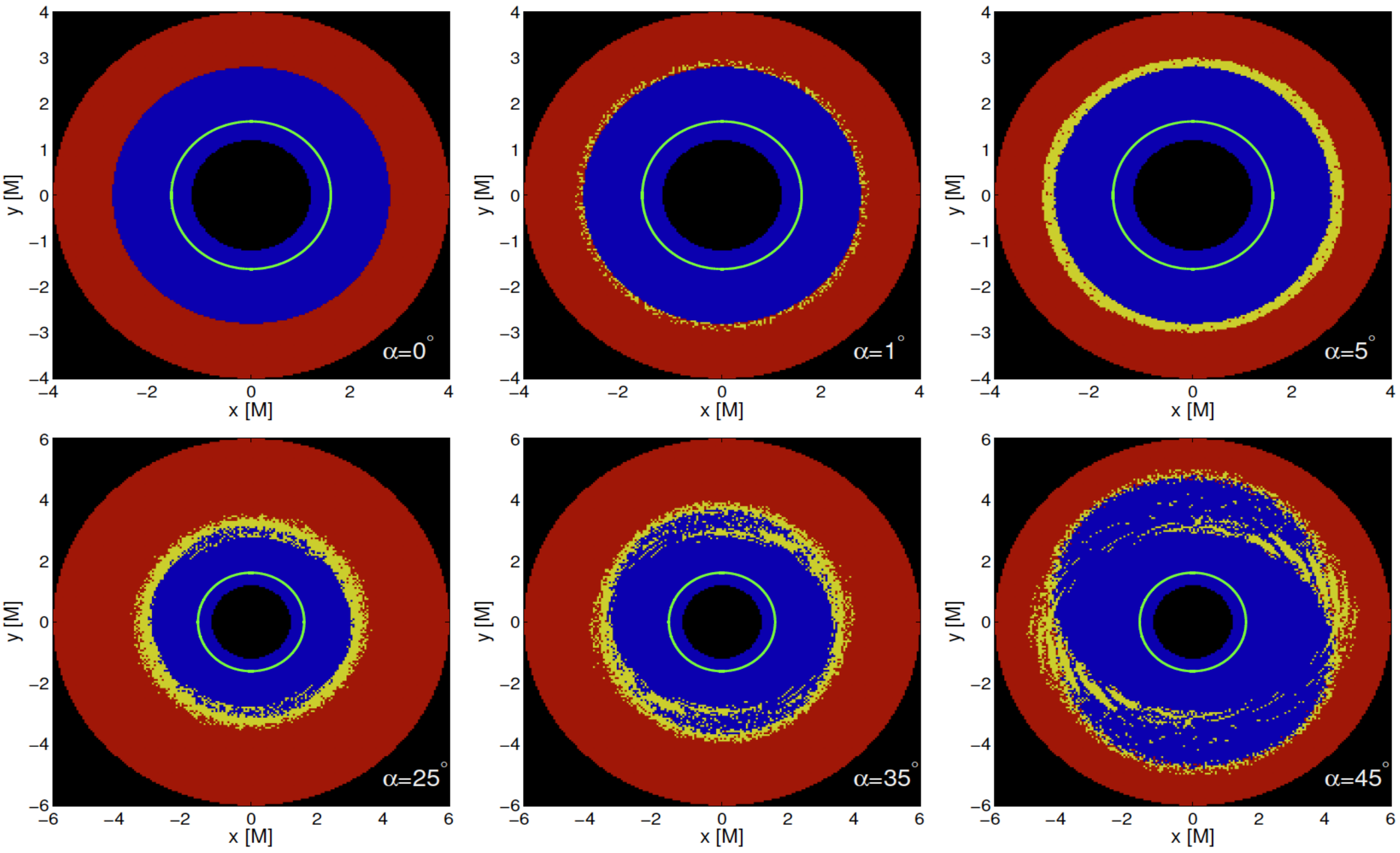

Figure 1. Different types of the trajectories launched from the equatorial plane (x, y) are plotted with respect to the magnetic inclination angle α. Color-coding: blue for plunging orbits, red for stable ones (bound to the black hole) and yellow for escaping trajectories. Green circle denotes the ISCO. Inner black region marks the horizon of the black hole. Parameters of the system are $a = 0.98$ and $qB = -5$. Magnetic field is inclined in the positive x-direction.

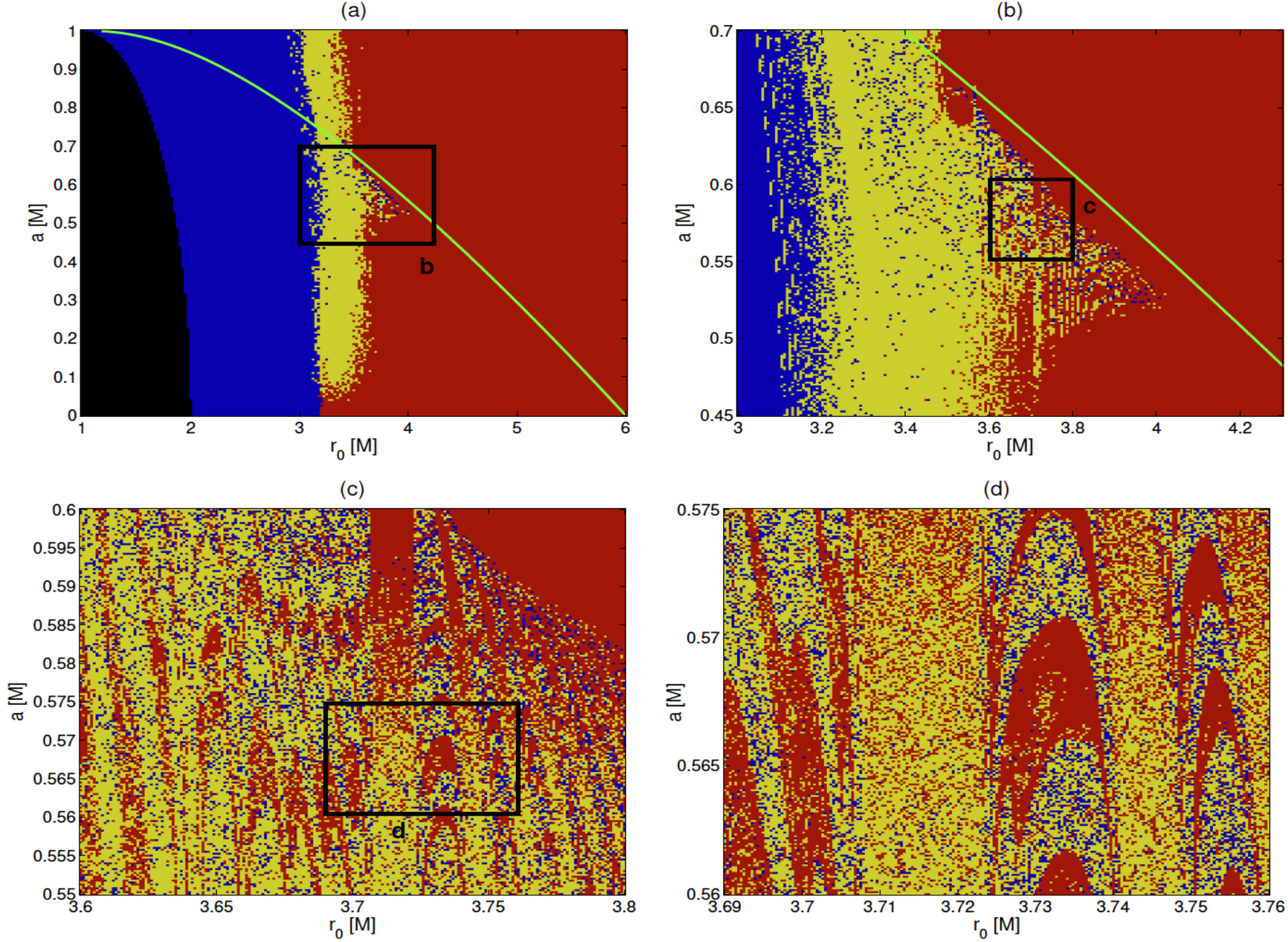

Figure 6. The structure of the escape zone ($qB = -4.1$, $\alpha = 14°$ and $\varphi_0 = 0$) in the relevant range of the spin parameter a and initial radius r_0 is explored. Going from the top-left to the bottom-right panel, the portions of the plots (marked by black rectangles) are magnified progressively in the subsequent panels revealing the complex structure. Green line represents the ISCO, black color shows the horizon of the black hole. Color-coding of trajectories as in Figs. 1-3.

Acceleration of particles escaping to large distance

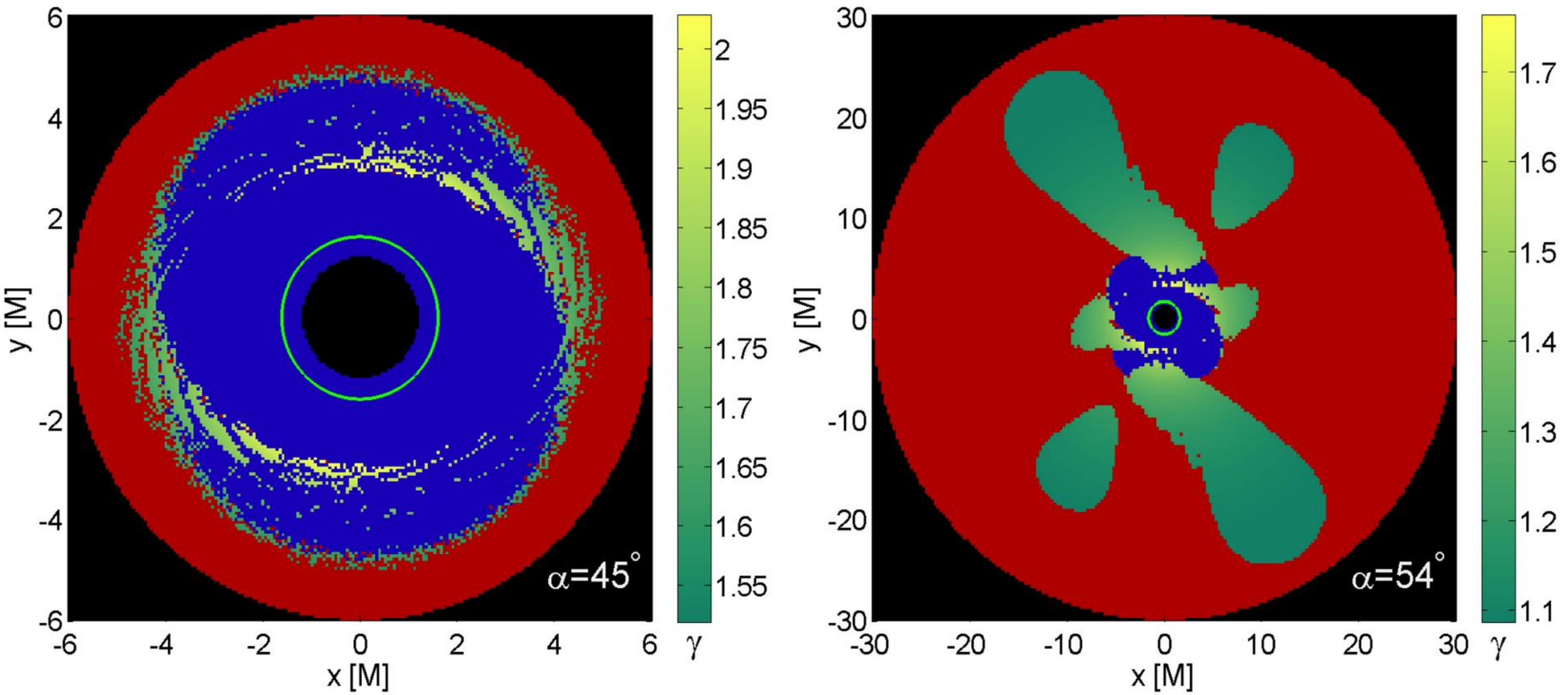

Figure 4. Final Lorentz factor γ of particles escaping from the equatorial plane is shown with the color-scale. Parameter choice as in Figs. 1-3 ($qB = -5$, $a = 0.98$). The field is inclined in the positive x-direction.

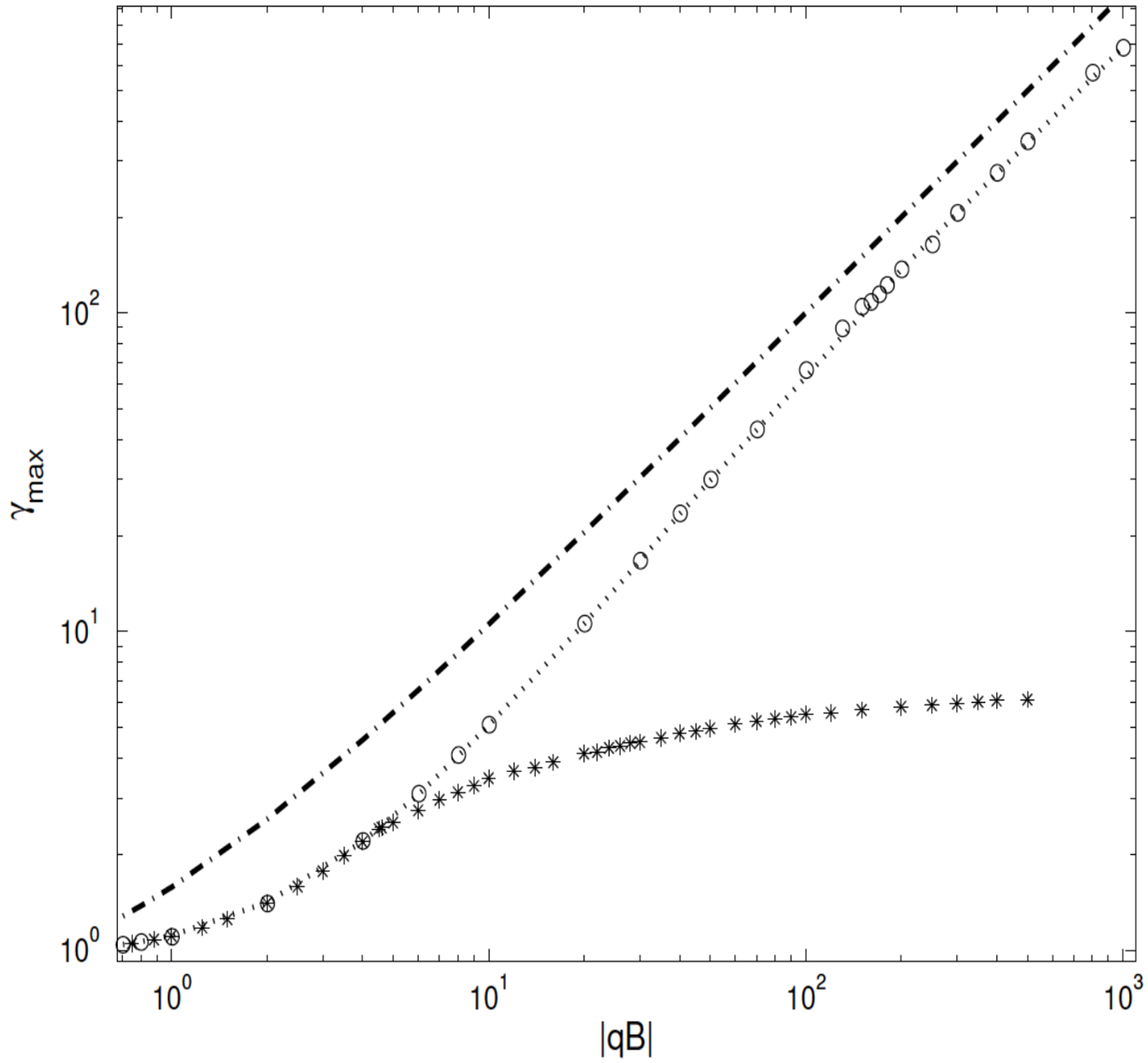

Figure 5. Maximal value of final Lorentz factor of escaping particles as a function of magnetization parameter $|qB|$. Circles denote values obtained numerically for trajectories in inclined magnetosphere ($B_x/B_z = 0.1$, i.e., $\alpha \approx 6^\circ$ with $\varphi_0 = \pi/2$), while stars show the aligned case ($B_x = 0$) analyzed in Paper I. Dashed line shows the expected value predicted by the Eq. (20) for numerically obtained value of $r_0^{\rm min}$ and dash-dotted is the theoretical maximum for $r_0 = r_+ = 1$.

To explore the effects of the black hole charge, we begin with the aligned (Wald) field.

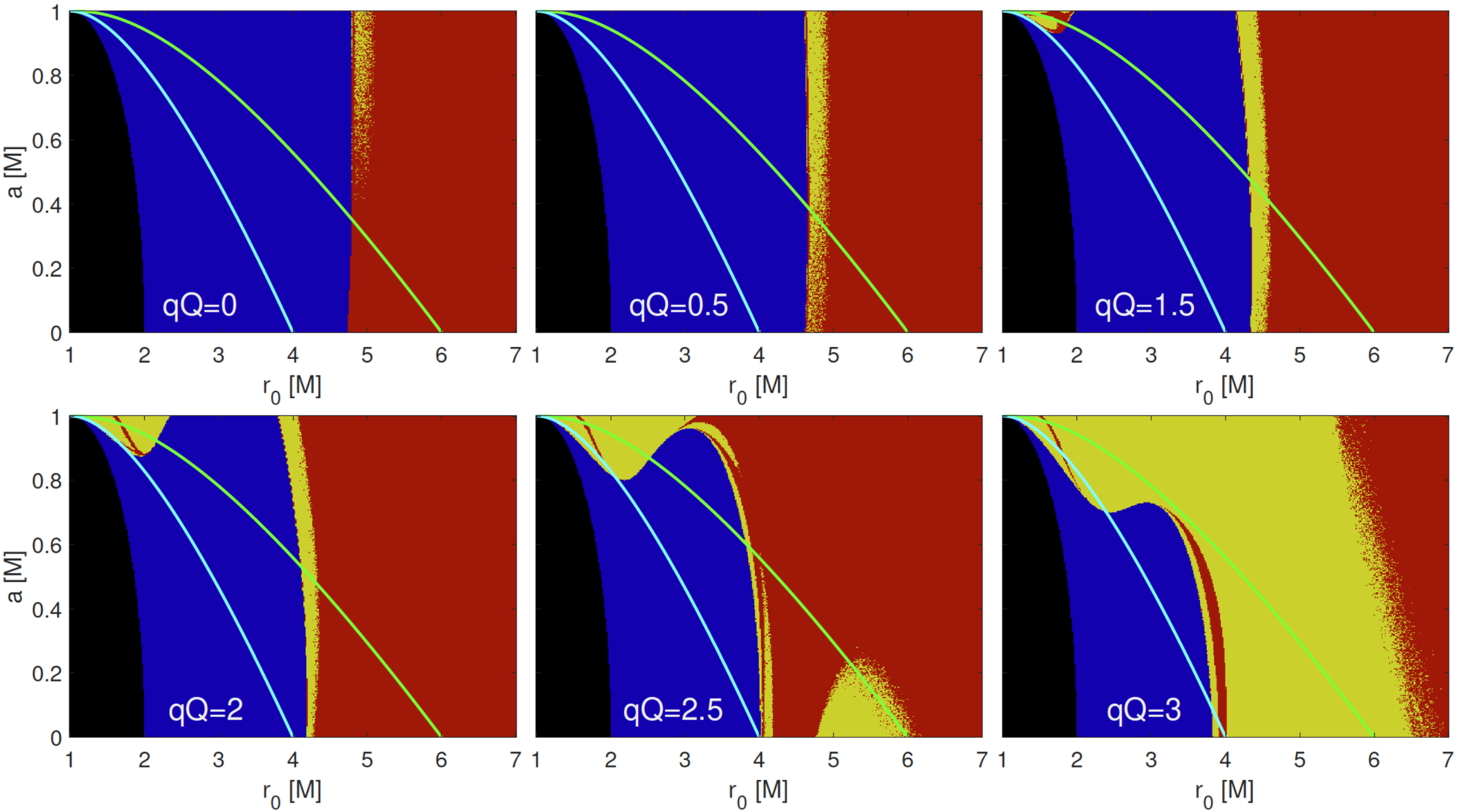

Figure 1. Evolution of escape zones of charged particles affected by the Coulomb repulsion of charged black hole. Color-coding of trajectories: blue for plunging orbits, red for stable ones (bound to the black hole) and yellow for escaping trajectories. The inner black region marks the horizon of the black hole. The green line denotes the ISCO of neutral particles, while the cyan line marks MBSO. Parameters of the system are $qB = -1$ and inclination $\alpha = 0$ while qQ varies as indicated.

Summary

We have computed the final Lorentz factor γ of escaping particles confirming that the highest γ is achieved in the innermost region of the primary escape zone (with the lowest allowed r_0). For a particular (realistically small; $\alpha \approx 6°$) value of inclination and fixed value of spin ($a = 0.98$), we searched for the maximal γ. Increasing the value of magnetization up to $|qB| = 10^3$ we confirmed that (unlike axisymmetric configuration) ultrarelativistic velocities with $\gamma \gg 1$ may be achieved. While the acceleration of the particle is actually powered by the parallel component B_z, the perpendicular component B_x acts as an extra perturbation which considerably increases the probability of sending the particles on escaping trajectories and allows the outflow also in cases which are excluded in the aligned setup.

References:

- Kopáček & Karas, The Astrophysical Journal, 966, 226 (2024)
- ---------"---------, The Astrophysical Journal, 900, 119 (2020)

Discussion slides & additional information

$$B_{\rm SI} = \frac{qB\ c_{\rm SI}}{q_{\rm SI}\left(\frac{M}{M_\odot}\right)1472\ \mathrm{m}}$$

Setting the specific charge of the electron, i.e., $q_{\rm SI} = -1.76 \times 10^{11}\,\mathrm{C\,kg^{-1}}$, we find that for the stellar-mass black hole of $M = 10\,M_\odot$, the corresponding magnetic field required for the acceleration to the relativistic velocity ($\gamma = 2$, $|qB| = 4$) reads $B_{\rm SI} = 4.63 \times 10^{-7}\,\mathrm{T}$. Large-scale magnetic fields observed in nonthermal filaments in the Galactic center are supposed to reach the same order of magnitude $B \approx 10^{-7}\,\mathrm{T}$ (Ferrière 2010), although more recent estimates are somewhat lower (Yusef-Zadeh et al. 2013). Nevertheless, stronger fields sufficient for the acceleration to ultrarelativistic velocities (setting $|qB| = 40$ in Equation (27) gives $B_{\rm SI} = 4.63 \times 10^{-6}\,\mathrm{T}$) might be encountered inside molecular clouds observed within the Milky Way (Han 2017).

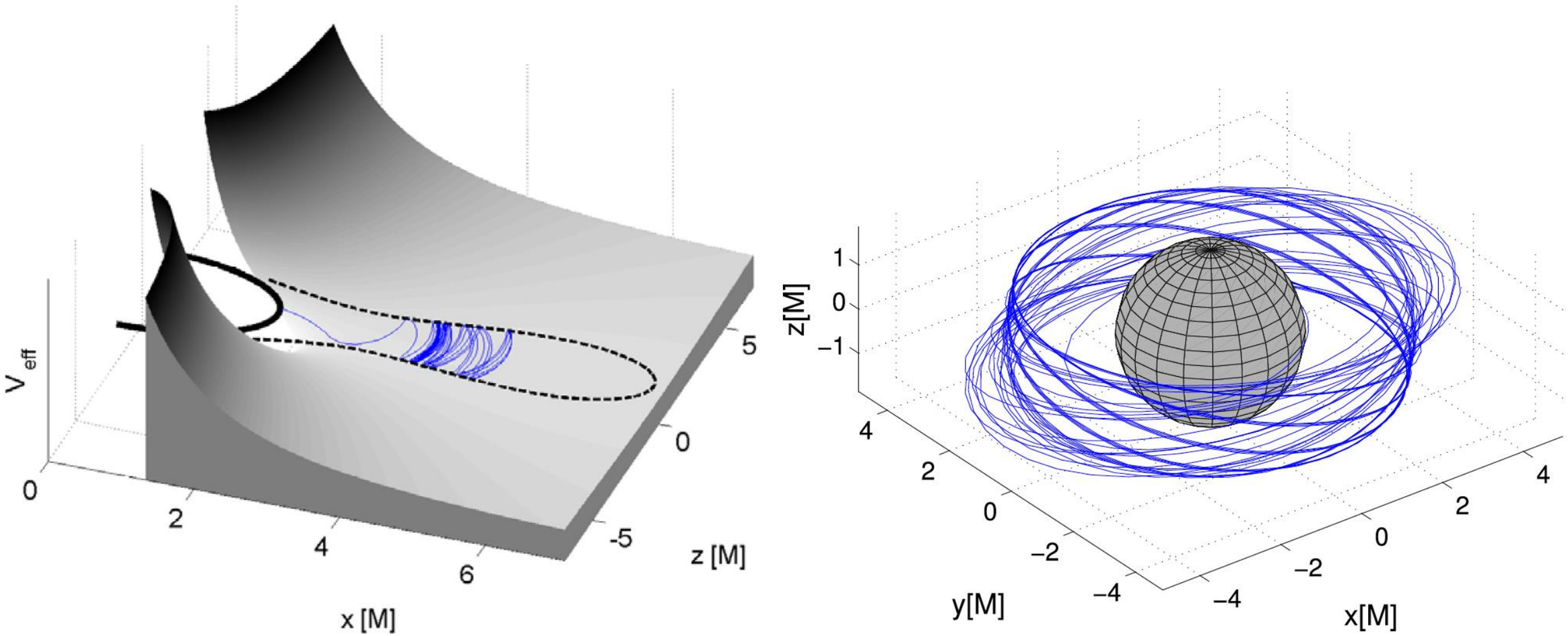

Example of an unstable plunging spherical orbit launched below the ISSO. The following parameters were employed: $r_0 = 4$, $Q^{1/2} = 0.75$, and $a = 0.5$.

Below the Innermost Stable Circular Orbit (ISSO)

Plunge from an unstable spherical orbit

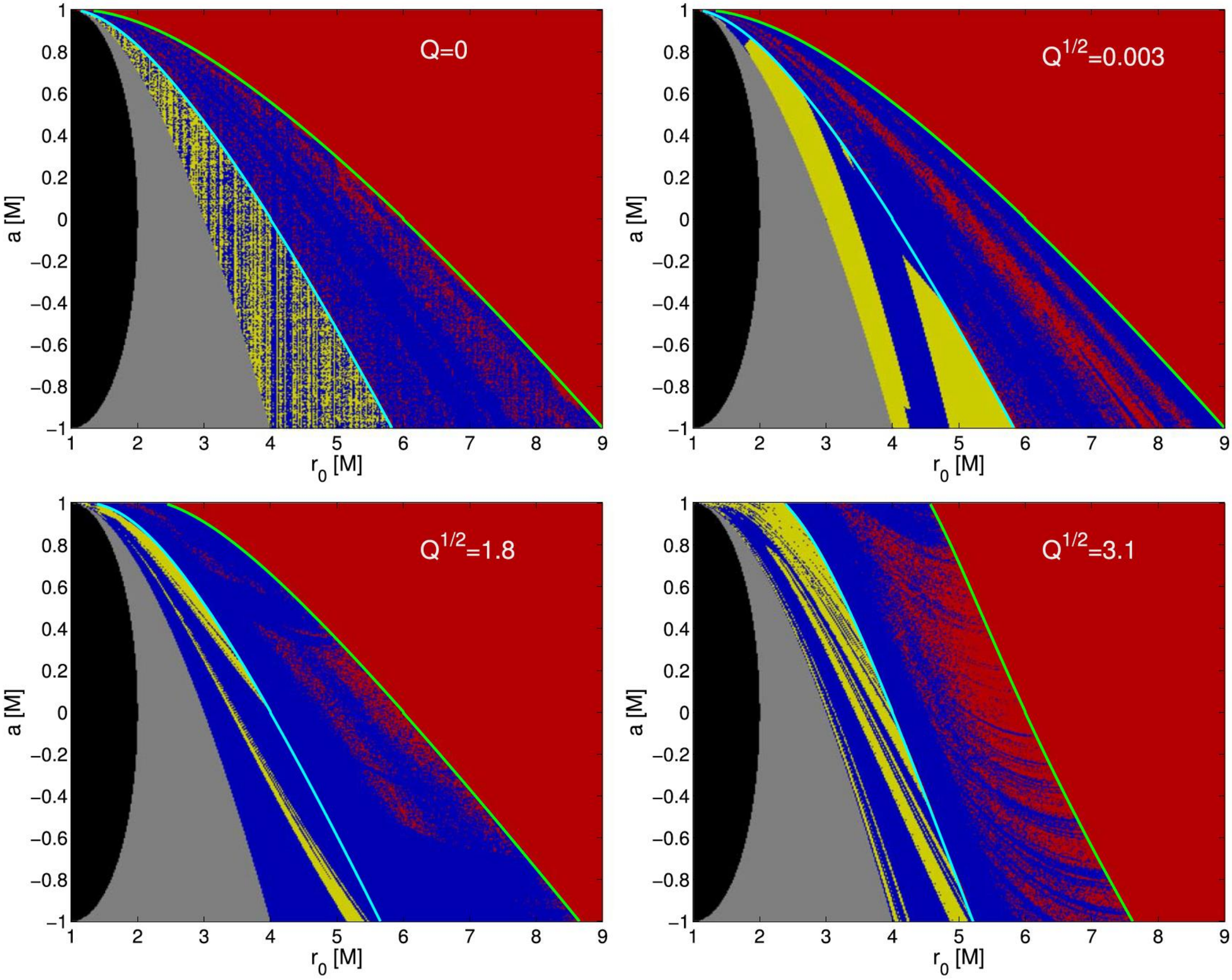

Figure 13. Escape-boundary plots with coordinates (r_0, a) and fixed values of the Carter constant. The spherical trajectories presented in these plots are color-coded as follows: yellow for escaping, red for bound, and blue for plunging orbits. Black indicates the black hole interior, and gray shows the regions above the horizon where spherical orbits cannot exist. The locations of the MBSO are shown by a cyan line and the location of the ISSO by a green line. Negative spin values correspond to counterrotating orbits.

Summary 2 - ISSO and MBSO

From the analysis performed in Section 3, we learn two basic facts regarding the stability of spherical orbits with given values of Q and a: (i) the radii r_s of the ISSO below which the spherical orbits become unstable and (ii) the radii r_b of the MBSO below which they become unbound (their energy exceeds the rest energy, i.e., $E > 1$ in dimensionless units) and may escape to infinity. Generally, $r_b \leqslant r_s$, while both radii only coincide in the case of corotating circular orbits ($Q = 0$) around a maximally spinning black hole for which $r_b = r_s = r_\pm = a = 1$.

References:

- Kopáček & Karas, The Astrophysical Journal, 966, 226 (2024)
- ---------"---------, The Astrophysical Journal, 900, 119 (2020)

The Hamiltonian $\mathcal{H}$ of a particle of electric charge q and rest mass m in the field A_μ and metric with contravariant components $g^{\mu\nu}$ may be defined as (Misner et al. 1973):

$$\mathcal{H} = \tfrac{1}{2} g^{\mu\nu}(\pi_\mu - qA_\mu)(\pi_\nu - qA_\nu), \tag{8}$$

where π_μ is the generalized (canonical) momentum. The equations of motion are expressed as:

$$\frac{\mathrm{d}x^\mu}{\mathrm{d}\lambda} \equiv p^\mu = \frac{\partial \mathcal{H}}{\partial \pi_\mu}, \quad \frac{d\pi_\mu}{d\lambda} = -\frac{\partial \mathcal{H}}{\partial x^\mu}, \tag{9}$$

where $\lambda \equiv \tau/m$ is dimensionless affine parameter (τ denotes the proper time). Employing the first equation we obtain the kinematical four-momentum as: $p^\mu = \pi^\mu - qA^\mu$, and the conserved value of the Hamiltonian is therefore given as: $\mathcal{H} = -m^2/2$. System is stationary and the time component of canonical momentum π_t is therefore an integral of motion which equals (negatively taken) energy of the test particle $\pi_t \equiv -E$. In the rest of paper we switch to specific quantities $E/m \to E$, $q/m \to q$ which corresponds to setting the rest mass of the particle $m = 1$ in the formulas.

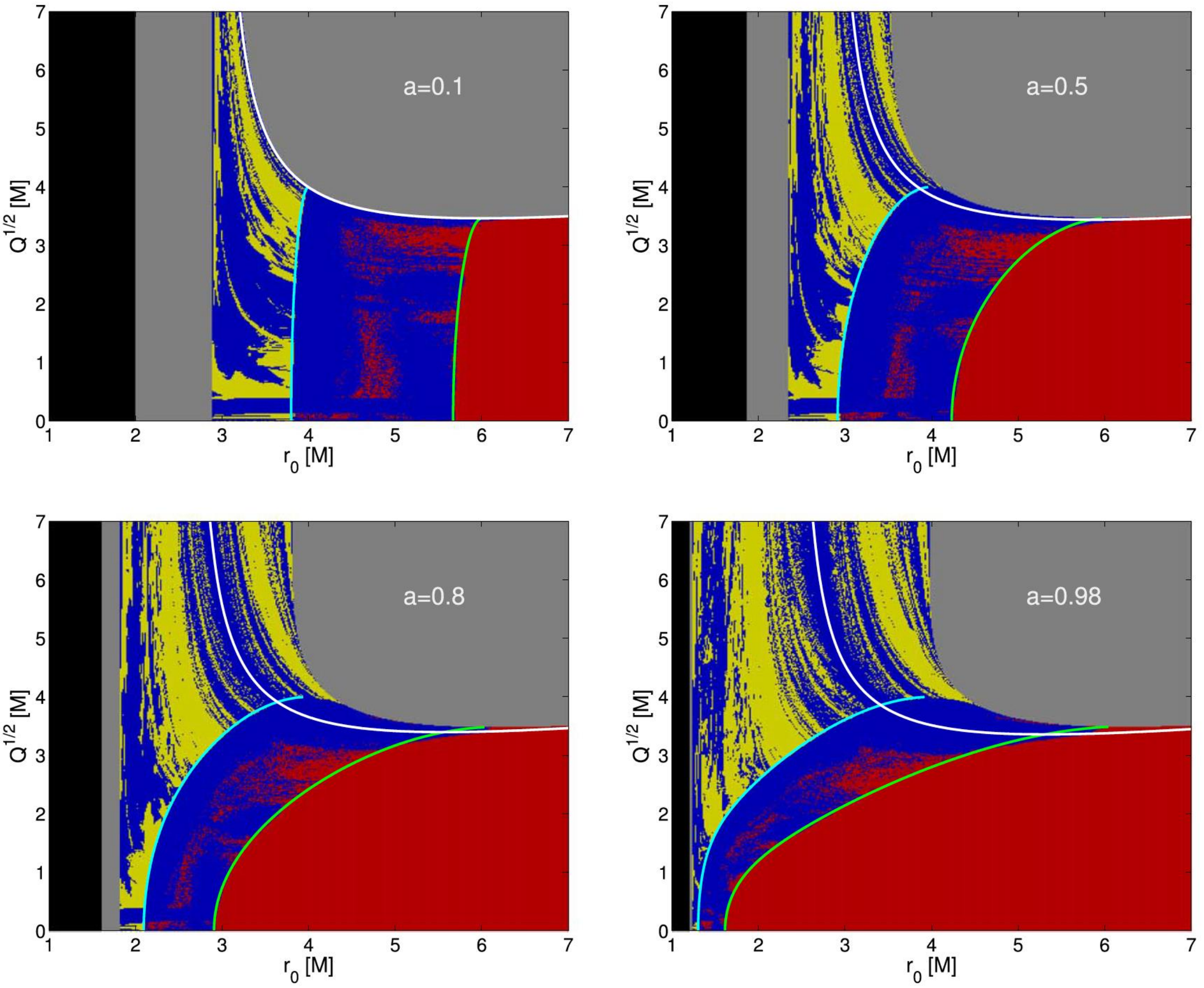

Figure 14. Escape-boundary plots with coordinates (r_0, $Q^{1/2}$) and fixed values of the spin parameter. The spherical trajectories presented in these plots are color-coded as in Figure 13. Besides the radii of the MBSO (cyan line) and the radii of the ISSO (green line), we also show the locations of polar orbits by a white line.